We are IntechOpen, the world's leading publisher of Open Access books Built by scientists, for scientists

4,800
Open access books available

122,000
International authors and editors

135M
Downloads

Our authors are among the

154
Countries delivered to

TOP 1%
most cited scientists

12.2%
Contributors from top 500 universities

CLARIVATE ANALYTICS BOOK CITATION INDEX INDEXED

WEB OF SCIENCE™

Selection of our books indexed in the Book Citation Index in Web of Science™ Core Collection (BKCI)

Interested in publishing with us?
Contact book.department@intechopen.com

Numbers displayed above are based on latest data collected.
For more information visit www.intechopen.com

3

Ion Transfer in Layer-by-Layer Films

Bin Wang and Ritesh N. Vyas

Abstract

The need for miniaturized devices has driven the exponential development of nanotechnology during the past two decades. One special field of paramount practical applications is electrochemical systems at the nano-scale. For successful development in such fields, an in-depth analysis of mass and/or charge transfer mechanism is highly desired. In such a system, mass transfer often takes the form of ion transfer, which can also be viewed as charge transfer. For example, in fuel cell development, the catalyst layer deposited on a polyelectrolyte membrane would demand higher ionic (protonic) conductivity. In the electrochemical sensors, the overall performance depends largely upon sensitivity of the thin films to recognize the analyte and the speed to communicate the resultant signals with the underlying electrodes. These phenomena are closely related to the (ionic) mass transfer within such films. A clear understanding of mass transfer in such an electrochemical system is the prerequisite for any significant progress in devices.

Fundamentally, three different types of mass-transfer phenomena exists for ionic species in electrolytes at electrodes: (1) diffusional transport under concentration gradient, (2) migration transport of oppositely charged ions under electric field of the electrode, and (3) convection transport due to physical stirring of the electrolyte. For electrodes modified with electroactive or redox films, the redox behavior is much more complicated. When the applied potential reaches the oxidation potential of the redox-active species in the film, the electron transfer from the electrode surface to the film is coupled with the simultaneous ionic transfer from electrolyte to the film for maintaining electro-neutrality. Thus, we observe two simultaneous mass-transfer processes at the same time and each one needs to be characterized individually.

A detailed study of mass-transfer within such films would first require conceptual understanding of the main characterization technique used. We will conduct a literature survey on various models used to characterize such mass transfer in layer-by-layer (LbL) films, and then propose a model for characterizing mass-transfer in LbL films that contain nanoparticles.

1. Introduction

Polyelectrolyte multilayers built through the layer-by-layer (LbL) method has been one of the most promising systems in the field of materials science.[1] Layered structures can be constructed by adsorbing various polyelectrolyte species onto the surface of solid or liquid material by means of electrostatic adsorption. The thickness of the adsorbed layers can be tuned precisely in the nanometer range. Materials of all forms besides polyelectrolytes, such

as organic and inorganic particles and crystals, biomolecules, lipids, and viruses, can be used to form diverse shapes with complicated stratified structures. Many factors influence the formation process of polyelectrolyte LbL films, including polymer type, molecular weight, concentration, deposition time, salt type and concentration, pH, and solvent composition.[2–5] Among them, salt concentration has shown to have predominant effect on the resultant film structure. Polyelectrolytes are the most thoroughly investigated class of substances in LbL studies; thus, the preparation parameters are well correlated with the film structures made of polyelectrolytes. Within an LbL film, the anionic and cationic polymer chains complex to each other to such a high degree that small salt counterions are usually absent. The intrinsic structure of the polyelectrolyte LbL films provides them unique properties in membrane separations.[6–11] In general, LbL films pertain no internal structures because of heavy interpenetration between adjacent layers, a result of the intrinsic nature of the charge compensation within the layers.[12,13] The LbL films can be viewed as amorphous and the parameters are not excessive when modeling the structures. Schlenoff *et al.* have employed electrochemical methods to evaluate the transport of redox-active ions across LbL films, addressing variables such as number of layers, ion charge, total ion concentration, and temperature.[14,15] The critical importance of the mechanism of internal charge balance within the layered structures in separating ions in solutions has been revealed by a quantitative treatment of equilibria.

The mass transfer phenomenon in polyelectrolyte LbL films has been well documented. Schlenoff *et al.* have employed electrochemical methods to evaluate the transport of redox-active ions across LbL films, addressing variables such as number of layers, ion charge, total ion concentration, and temperature.[14-17] On the basis of the observed increases of limiting current with increases in the external salt concentration, they proposed that the diffusion of the probe ion in the film is described as hopping between "exchange sites" created within the film by the supporting electrolyte. The strong attenuation of the current is explained as a combination of a low diffusion coefficient and a low concentration of the electroactive ion in the film. The decrease in permeability with the number of layers is attributed to a decrease in the concentration gradient in the film due to an increase in film thickness. However, this and many other mass-transport studies in LbL films have been accomplished through different techniques like cyclic voltammetry and chronoamperometry.[10,18-21] In this study, we plan to systematically investigate the mass transfer phenomena in LbL thin films through the electrochemical impedance spectroscopy (EIS). EIS has been widely used as a versatile technique to characterize interfacial and transport properties of polymer films adsorbed on surface of an electrode.[22] The estimation of parameters such as diffusion coefficient and electron transfer rate constant can explain the kinetics at interfaces, thus this technique becomes relatively easy and accurate as compared to other techniques.[23–25] In applying EIS for electrochemical system analysis, an important consideration is to fit experimental data to a suitable model. The use of EIS to study LbL films has become more common once LbL films find potential future in the field of bio-sensors and electrochemical sensors.

An early study shows the use of EIS in studying membrane resistivity and capacitance where phospholipid bilayers were deposited on LbL polyelectrolyte surface.[26] EIS has been used to characterize the stability and insulating properties[27-30] of LbL films that are stabilized by different approaches like cross-linking and thermal conversion. The charge transfer resistance and film resistance are obtained directly from the fitting of experimental

impedance spectrum to Randle's equivalent circuits (vide infra) by simulation software. The films were exposed to different conditions of *p*H and temperature and insulating or corrosion resistant properties of the films were observed by variation in the calculated resistances. Self-assembled monolayers[31] and multilayers of polyelectrolytes have been widely studied for analyzing permeability towards ionic diffusion at various stages of LbL deposition.[32-34] Zhao *et al.* have demonstrated potential applications of LbL assembly in preparing hybrid compounds containing Prussian-blue (PB) redox-mediators for future applications in bio-sensors.[35] The authors used PB nanoparticles protected by PDDA in alternating fashion with negatively charged glucose oxidase. The modified electrodes were able to catalyze the electro-reduction of hydrogen peroxide formed from the enzymatic reaction at a lower potential than bare electrodes. EIS has been one of the primary techniques to characterize the electronic communication of the analyte with the modified electrodes.[36-41] Recently, Calvo *et al.* demonstrated the use of EIS in measuring ionic diffusion coefficients in pyridine derivatized (PAH│PSS) multilayer films.[42] Other advances also include EIS studies for explaining catalytic and charge storage efficiencies of LbL assembled nano-scale species such as gold,[43-45] titanium dioxide,[46] vanadium pentoxide,[40] polyoxometalates,[47] and carbon nanotubes.[48] Thus, EIS has been widely applied in extracting absolute values of the electrochemical parameters governing electronic and ionic transfer in LbL films. However, in most of the cases studied above, the experimental data has been directly fitted to an equivalent circuit proposed by the researchers to explain the electrochemical phenomena in LbL films. In other words, the conceptual modeling of LbL films that can directly relate the microstructure of the film with the experimental EIS spectrum has been omitted. Silva *et al.* have performed such EIS modeling in LbL films of polyelectrolytes[49,50] as well as gold nanoparticles.[38,51] Here, we first review the proposed models for gaining further insight in EIS modeling of LbL films. Followed, we will develop an EIS model to describe the mass transfer in functional LbL films. We then will analyze experimental results by using such modeling.

Capillary Membrane Model (CMM)

The CMM model is developed to consider progressive reduction of the active area of the electrode with the increase in deposition of the films. The diffusion impedance of partially blocked electrodes is often modeled by assuming that the ensemble of active sites behaves as an ideal array of microelectrodes (Figure 1).[52] These models can be adapted for polyelectrolyte multilayers having capillaries (or preferential transport paths) and areas through which transport is hindered or very unfavorable. At the initial stages of the deposition effective coverage of the electrode for these films is small (Figure 2.1). A formation of pin-holes resulting from the disordered arrangement of polyelectrolyte chains is assumed such that these pinholes also persist during the sequential assembly of the polyelectrolyte layers, although their area is progressively reduced Eventually, at larger number of layers, the remaining electroactivity may still be associated with the previously formed pin-holes because these continue to be active-sites were the film is less dense but now redox-species has to diffuse through external layers before reaching the capillary (Figure 2.2). Let us assume that species **Ox** and **R** are electroactive species residing in the film. For such a non-linear diffusion Finklea *et al.*[52] have compared the problem with an electron transfer step of species **Ox** and **R** within the film with preceding and succeeding chemical steps of redox couple **A** and **B** as follows:

$$\mathbf{A} \underset{k_2}{\overset{k_1}{\leftrightarrow}} \mathbf{O_x} \tag{1}$$

$$\mathbf{O_x} + e^- \leftrightarrow \mathbf{R} \tag{2}$$

$$\mathbf{R} \underset{k_1}{\overset{k_2}{\leftrightarrow}} \mathbf{B} \tag{3}$$

For a blocking layer with coverage of θ, (1- θ) represents the area fraction of microelectrodes. When (1- θ) is less than 0.1, then coverage θ and the radius r_b of inactive area surrounding the active site in above figures are related by the following relation

$$1-\theta = \frac{r_a^{\,2}}{r_b^{\,2}} \tag{4}$$

Thus for disk shaped pin-holes, the rate constants have been expressed:

$$\frac{k_1}{k_2} = \frac{(1-\theta)}{\theta} \tag{5}$$

$$k_1 + k_2 = \frac{\left[\frac{D}{4r_b^{\,2}}\right]\left[\frac{\theta}{(1-\theta)^2}\right]}{\left(0.3(1-\theta)^{-1/2}\right)^2} \tag{6}$$

Where D is the diffusion coefficient of redox-species.
The real and imaginary components of the faradaic impedance for coupled reaction schemes have been obtained as:

$$Z_{re} = R_{ct}\frac{\theta}{(1-\theta)} + \frac{\sigma}{\sqrt{\omega}} + \left(\frac{\sigma\theta}{(1-\theta)}\right) \tag{7}$$

$$Z_{img} = \frac{\sigma}{\sqrt{\omega}} + \left(\frac{\sigma\theta}{(1-\theta)}\right) \tag{8}$$

where q is the average time taken for diffusion of the oxidized and reduced species. The last two terms in above equations depict the diffusion process in the system. Based on the above equations Silva *et al.*[49] have extracted an expression solely for diffusion impedance in polyelectrolyte films as under:

$$Z_d^{\,(c)} = \sum_k \frac{\sigma_k^{\,(c)}}{\sqrt{\omega}}\left(1 + \frac{\theta}{(1-\theta)} + j + \frac{j\theta}{(1-\theta)}^{1/2}\right) \tag{9}$$

The Warburg parameter σ and diffusion coefficient D can be obtained according to the following equation:[53]

$$\sigma = \frac{RT}{n^2 F^2 A\sqrt{2}}\left(\frac{1}{c_{\mathrm{Ox}}{}^{*}\sqrt{D_{\mathrm{Ox}}}} + \frac{1}{c_{\mathrm{R}}{}^{*}\sqrt{D_{\mathrm{R}}}}\right) \tag{10}$$

If we consider the values for concentrations and diffusion coefficients of oxidized (c_o^*) and reduced species (c_R^*) to be same as those in the bulk then we can assume $c_{\mathrm{Ox}}{}^{*} = c_{\mathrm{R}}{}^{*} = c$ and $D_{\mathrm{Ox}} = D_{\mathrm{R}} = D$ and we get

$$\sigma_{\mathrm{k}}{}^{(c)} = \frac{\sqrt{2}RT}{n^2 F^2 A D_k^{f\,1/2} c_k^f} \tag{11}$$

where, the concentration of species k (k = 1 for $[Fe(CN)_6]^{4-}$ and k = 2 for $[Fe(CN)_6]^{3-}$) in the vicinity of the film surface. c_k^f is equal to its concentration in the bulk solution, c_k^S. The equivalent circuit for such a system is shown in Figure 3**.**

Homogeneous Membrane Model

Silva and co-workers studied the above model for the effects of supporting electrolyte and temperature on impedance response.[49,50] PSS | PAH multilayers have been characterized with EIS, however, a third situation is added where the number of layers become so large that the polyelectrolyte multilayers become practically homogeneous as shown in Figure 4. The film has also been modeled as a homogeneous membrane where the increase in the number of layers leads to an increase in the thickness L of the film, a decrease in the concentration gradient, and then a decrease in the current. This tendency, for the decrease in the permeability with the increasing layers may not occur when the last layer deposited and the electroactive species have opposite charge. In this case the decrease in concentration gradient associated with the increase in film thickness may be compensated by an enhanced inclusion of the species in the film. The film-solution interface is considered to be in electrochemical equilibrium. The diffusion coefficient D_k^f and the partition coefficient K_k of species k are allowed to vary with the number of layers. For a thicker homogeneous film, the diffusion is predicted by assuming that diffusion layer thickness l is finite and in the case of homogeneous polymer films is equal to the film thickness L. The diffusion impedance in this case has been derived as

$$Z_{\mathrm{k,d}}{}^{(m)} = \frac{\sigma_{\mathrm{k}}{}^{(m)}}{\sqrt{j\omega}} \frac{\tanh(a_{\mathrm{k}}\sqrt{\omega}) + K_{\mathrm{k}}\sqrt{D_{\mathrm{R}}}}{1 + b_{\mathrm{k}}\tanh(a_{\mathrm{k}}\sqrt{\omega})} \tag{12}$$

$$\sigma_{\mathrm{k}}{}^{(m)} = \frac{\sqrt{2}RT}{n^2 F^2 A D_k^{f\,1/2} c_k^f(0)} \tag{13}$$

where,
$$a_{\mathrm{k}} = \frac{L}{\sqrt{2D_{\mathrm{k}}{}^{f}}}(1+j) \tag{14}$$

LbL Assembled Films of (PMo_{12} | PDDA)

It is clear from the above study that modeling of ionic and electronic conductivity in LbL films by EIS would be a significant research contribution. Recently, Hammond *et al.* separately measured ionic and electronic conductivities in LbL assembled conducting polymer films by de-doping the conducting polymer to minimize the contribution from electronic conductivity.[54] However, EIS modeling of LbL films to measure ionic and electronic conductivites individually has not been accomplished till date. Moreover, LbL films containing nanoparticles (NPs) are much less studied in this respect. Nanoparticles with dimension in the 1-100 nm range can be assembled with polyelectrolytes through the LbL method.[55] Both ionic and van der Waals interactions have significant contributions to depositing NPs, most water-based and highly charged, into LbL films. A combination of strong electrostatic attraction and firm binding to the surface polyelectrolyte layer makes the adsorbed NP layer thermodynamically more preferable than the dissolved state. Nanoparticles such as CdSe, TiO_2, SiO_2, and gold are among the well studied. These NPs are highly interesting for applications ranging from light emitting diodes to photovoltaics to sensors and to semiconductors. One particular field is electrochemical reactions in which NPs have widely been employed as catalysts due to the hugely enhanced surface areas and hence higher catalytic efficiencies.[56-58] The combination of the ultrathin feature of LbL films and the high surface area of NPs seems a highly desirable architecture for developing new catalysis systems. A fundamentally critical aspect in understanding electrochemical reactions within the NP-embedded LbL films is the mass transfer phenomenon through the membrane. The proposed study will deal with the ion diffusion in a thin film that is regulated not only by electrostatic forces between the composing polyelectrolyte chains and NPs, but also by the geometric constraints brought by the particulate matter. The knowledge obtained from such a study has both very broad industrial application potential and is the key to understanding other thin membrane systems immensely encountered in biology.

To successfully establish the preparation parameters in constructing NP-containing LbL films, we can maneuver two important parameters in such a process, NP concentration and solution ionic strength. We choose polyoxometalate (POM) clusters as the NP component to probe the LbL deposition parameters. Polyoxometalates are a well-known class of ångström-scale anionic clusters with much diversity in size, composition, and function. Their interesting properties include the high stability of most of their redox states, the possibility to tune their redox potentials by changing the heteroions and/or the addenda ions without affecting their structure, the variability of the transition metal cations which can be incorporated into the hetero-polyoxometalate structure, and the possibility of multiple electron transfer.[59] Because most POM clusters are water soluble, they are ideal candidates for the LbL assembly technique. There has been an increasing interest in constructing POM thin films through the LbL process.

We attempt to find a generic fabrication rule that applies to most POM clusters.[60] In the study, we used Keggin type POM clusters to study their layer-by-layer deposition behavior. We found that POMs can be adsorbed onto LbL assemblies from concentration range 0.1 to 5 mM. We use two situations, without added salt and with added salt (0.1 M). When the

deposition was performed without added salt, the ionic strength of a solution was at a few mM scale originated from the counter ions and HCl added to adjust the pH. Under this condition, POM clusters adsorb at sub-monolayer coverage. The cluster concentration shows limited influence on the deposition process. When the cluster concentration was increased from 0.1 mM to 5 mM, a 50-fold increase, the coverage merely increased by ~15-30% for both POM species. When NaCl is added to the deposition solutions, the results are more complex. For depositions from a low POM concentration, the adsorption is still at the about-monolayer level. But when POM concentration is above 1 mM, multilayer structures start to form.

Here, we study the ionic diffusion phenomena of a redox couple in LbL assembled PMo_{12} films. It is our interest to observe the effects of varying porosity and loadings of the film on the diffusion process of redox-active ions. We first construct an EIS model that can be applied to POM films with varying loading concentrations. We find diffusion coefficients for the ferrocyanide redox couple to understand the effect of electrostatic attraction/repulsion between redox-probe ion and the microstructure of the LbL films. The microstructure of the films as interpreted with EIS has been compared with that obtained from cyclic voltammetry (CV) measurements.

2. Methodology

As stated in the Introduction, EIS has been widely used as a versatile technique to characterize interfacial and transport properties of polymer films, organic-inorganic coatings, and self-assembled monolayers adsorbed on surface of an electrode. The estimation of parameters such as diffusion coefficient and electron transfer rate constant that can explain the kinetics at interfaces becomes relatively easy and accurate as compared to other techniques. The typical Nyquist plots for polyelectrolyte films exhibit a characteristic semicircle at higher frequencies corresponding to kinetic control, and a straight line at lower frequencies (slope ~ 1) corresponds to mass-transfer control. A Randle's equivalent circuit model can be used in case of self-assembled films with or without modifications.[28] Briefly, the circuit consists of solution resistance R_s in series with the parallel combination of double-layer capacitance (C_{dl}) and charge-transfer resistance (R_{ct}) with Warburg impedance (Z_w) in series (Fig. 1). The equations for a simple Randle's circuit can be directly used for calculations if Warburg line on Nyquist plot has a slope close to 1. In our case, diffusion coefficient for $Fe(CN)_6^{3-/4-}$ redox species were calculated. The real and imaginary values for impedance for an ideal Randle's circuit (Figure 5) can be given as:[39]

$$\left(Z_{re}\right)_1 = R_s + \frac{R_{ct} + \sigma\omega^{-1/2}}{\left(C_{dl}\sigma\omega^{1/2} + 1\right)^2 + \omega^2 C_{dl}{}^2\left(R_{ct} + \sigma\omega^{-1/2}\right)^2} \tag{15}$$

$$\left(Z_{im}\right)_1 = \frac{\omega C_{dl}\left(R_{ct} + \sigma\omega^{-1/2}\right)^2 + \sigma\omega^{-1/2}\left(C_{dl}\sigma\omega^{1/2} + 1\right)}{\left(C_{dl}\sigma\omega^{1/2} + 1\right)^2 + \omega^2 C_{dl}{}^2\left(R_{ct} + \sigma\omega^{-1/2}\right)^2} \tag{16}$$

where ω is the radial frequency and σ is the Warburg parameter. If the deposited film behaves as an ideal capacitor on the electrode, then we always observe a vertical line with a unity slope in low-frequency region.[9] For the high frequency region, the intercept with real impedance axis would also give the accurate values for solution resistance R_s of Figure 5. However, the charge transfer resistance R_{ct} and double layer capacitance C_f only describe the resistance and capacitance provided by the electrochemical double layer at the interface, an ideal semi-infinite diffusion. In our study of POM films, the experimental data show depressed semi-circles in high frequency region with a slight deviation from unity slope in lower frequency region. Thus, a resistance to the movements of redox ions inside and out of the deposited film needs to be addressed to the circuit along with the charge transfer resistance. Adding a film resistance (R_f) in parallel to double layer capacitance in the circuit has been employed for self-assembled monolayer. Silva and coworkers dealt with this problem differently and employed two models in the case of polyelectrolyte films with increasing thickness.[49,50] Here, the Randle's circuit was modified by addition of two more resistances, namely film resistance R_f offered by multilayers and R_m due to ohmic conduction within the film. The films in their studies exhibited non-linear diffusion; in contrast, our films demonstrate semi-infinite diffusion patterns. Here, we adapt the same Randle's circuit as in Figure 2.1.3.5.3, but add two more elements to the circuit to define the properties of film: film resistance (R_f) and film capacitance (C_f). Equations (15) and (16) are thus modified as

$$(Z_{re})_2 = R_s + \frac{\dfrac{R_f + (Z_{re})_1}{(\omega C_f)^2}}{[R_f + (Z_{re})_1]^2 + \left[(Z_{img})_1 - \dfrac{1}{\omega C_f}\right]^2} \tag{17}$$

$$(Z_{img})_2 = R_s + \frac{\dfrac{(Z_{img})_1}{(\omega C_f)^2} + \dfrac{(Z_{img})_1^2 - (Z_{re})_1^2 - R_f (Z_{re})_1}{\omega C_f}}{[R_f + (Z_{re})_1]^2 + \left[(Z_{img})_1 - \dfrac{1}{\omega C_f}\right]^2} \tag{18}$$

where, $(Z_{re})_2 = Z'$ is the real component of the modified Randle's circuit, and $(Z_{re})_2 = Z''$ is the imaginary component of the circuit. After modifying the circuit, we can develop equations to calculate the diffusion coefficients for thin film samples. At low frequencies ($\omega \rightarrow 0$), Eq. 17 and 18 become:

$$Z' = R_s + R_f + R_{ct} + \sigma\omega^{-1/2} \tag{19}$$

$$Z'' = \sigma\omega^{-1/2} + 2\sigma^2 C_{dl} + 4\sigma^4 C_{dl}^2 C_f - R_f^2 C_f - R_{ct}^2 C_f \tag{20}$$

From Eq. 19, the plot of Z' vs. $\omega^{-1/2}$ gives slope = σ and intercept = $(R_s + R_f + R_{ct})$. The intersection of a Nyquist plot with x-axis gives the values for solution resistance R_s that can be used to calculate R_{ct} from the intercept values. The Warburg parameter σ and diffusion coefficient D can be obtained according to Ref. 61:

$$\sigma = \frac{RT}{\sqrt{2}n^2F^2A}\left(\frac{1}{D_{\mathrm{Ox}}^{1/2}c_{\mathrm{Ox}}} + \frac{1}{D_{\mathrm{red}}^{1/2}c_{\mathrm{red}}}\right) \quad (21)$$

where n is the number of electrons transferred (in this case 1), F is Faraday's constant (96485 C·mol^{-1}), A is the electrode area (1 cm^2), R is gas constant (8.314 J·mol^{-1}·K^{-1}) and T is room temperature (298 K). Assuming diffusion coefficients $D_{\mathrm{ox}} = D_{\mathrm{red}} = D$ and concentrations $c_{\mathrm{ox}} = c_{\mathrm{Red}} = c_{\mathrm{bulk}}$ we get:

$$D = \left(\frac{\sqrt{2}RT}{n^2F^2A\sigma c_{bulk}}\right)^2 \quad (22)$$

This equation resembles the one obtained by Bobacka and coworkers.[40] From Eq. 2, the calculated values for diffusion coefficients become approximation values and are called apparent diffusion coefficients.

3. Experimental Section

Chemicals. 3-aminopropyltriethoxysilane (APTES), phosphomolybdic acid hydrate (PMO_{12}, reagent grade) and poly(diallyl dimethyl ammonium chloride) (PDDA; M_W 250,000) were purchased from Sigma-Aldrich and their aqueous solutions were filtered immediately before use. Potassium ferricyanide, potassium ferrocyanide and sodium phosphate were purchased from Malinckrodt. The nanopure water used for all experiments was purified by Barnsted Nanopure II purification system. The resistivity was about 18 MΩ/cm. The PDDA solution (10 mM, pH 2.5) was used with or without the addition of 0.1 M NaCl while POM solutions are explained in Results sections.

Preparation of ITO electrode. Indium tin oxide (ITO) coated glass slides (Sigma-Aldrich, 80–100 Ω) were cleaned and coated with a monolayer of APTES according to published procedures.[62,63] Briefly, freshly cut ITO slides (25 × 10 × 1 mm) were consecutively sonicated in acetone, base-bath (10% KOH in isopropyl alcohol) and nanopure water for 20 minutes each. Afterwards, the slides were given electrochemical cycling (-200-700 mV) in 0.1 M HCl solution until the characteristic ITO curve was obtained. The slides were then dipped in APTES (2 v %, methanol) solution overnight to form a cationic monolayer. The slides were sonicated for 5 minutes in methanol solution before the deposition of multilayers.

Preparation of the multilayer. PMO_{12} | PDDA multilayer films were deposited according to our recently published procedure.[60] APTES modified ITO slides were dipped in PMO_{12} solution (10 min) and PDDA solution (10 min) in an alternating fashion for 10 consecutive times, between each dipping the slides were exposed to three consecutive water baths for 5 seconds each.

Electrochemical cell and the measurements. Electrochemical measurements were conducted on a Voltalab 10 PGZ 100 Potentiostat equipped with VoltaMaster 4 Electrochemical Software version 2.10. A conventional three-electrode setup was used. The working electrode was the ITO slide modified with self-assembled films, while a platinum wire was used as the counter electrode. An Ag/AgCl (3 M KCl) reference electrode was used for all measurements. EIS measurements were performed within the frequency range 1 Hz–100 kHz with amplitude of the applied sine wave potential as 10 mV and applied dc potential as

220 mV. A mixture of 5 mM concentration of $K_3[Fe(CN)_6]$ and $K_4[Fe(CN)_6]$ (1:1) in 25 mM sodium phosphate solution was used as redox probes.

4. Results and Discussion

Preparation and characterization of $(PMo_{12}/PDDA)_{10}$ films. $(PMo_{12}|PDDA)_{10}$ films (samples **1-4**) were prepared according to the conditions in Table 1. Cyclic voltammetry (CV) was used to characterize the electrochemical behavior of the films. A recent study has shown that electrostatic attraction/repulsion between terminating layer in multilayer assembly and solubilized charged redox species play an important role in diffusion as well as electron transfer at the interface.[43] A multilayer assembly with a layer of negatively charged nanoparticles on the top has proved to be barrier for redox processes of negatively charged couples such as $[Fe(CN)_6]^{3-/4-}$.[38,45,46] However, we observe a different behavior when the samples in this study are coated with PMo_{12}^{3-} clusters. The CV curves for $(PMo_{12}|PDDA)_{10}$ multilayers, in which a PMo_{12} layer was the outmost layer, were obtained when $[Fe(CN)_6]^{3-/4-}$ was used as the redox couple. CV curves (Figure 7) for sample **1** at increasing scan rates (10-70 mV·s^{-1}) show a linear increase in redox peak currents with the square roots of their corresponding scan rates. Similar behavior has been observed with samples **2**, **3**, and **4**. The CV shapes are not broad or having a plateau, indicating that the current is not originated from an array of microelectrodes nor there is a slow diffusion through films.[64,65] Combined with Figure 8, there seems like a semi-infinite linear diffusion in the film for each sample. Figure 8 shows the comparison of redox curves for samples **1–4** when the scan rate was 100 mV·s^{-1}. We observe anodic peak at ~300 mV and cathodic peak at ~–50 mV for all samples, with peak-to-peak separation $\Delta E_p = 350 \pm 50$ mV indicating quasireversible voltammograms. The difference in peak-to-peak separation ΔE_p suggests variation in film structure or charge.[23] The increase in the peak currents for films made with higher ionic strengths (samples **2** and **4**) may suggest an increase in the permeability of the films due to increased porosity. The high permeability may be originated from a moderate delamination of films and less-stratified microstructure. Compared to the PMo_{12} surface coverage trend,[60] the diffusion of $[Fe(CN)_6]^{3-/4-}$ couple into the multilayer assembly seems independent of the PMo_{12} loading.

Mass transport analysis of $(PMo_{12}/PDDA)_{10}$ films. Figure 9 illustrates the fits obtained with the modified Randle's circuit to impedance data for samples **1–4**. The fitting of the data to the equivalent circuit (Figure 6) was performed by using Zview software. The parameter values, given in Table 2, agree well with the EIS experimental data. In Figure 9, the Nyquist plots for samples **1–4** exhibits a characteristic semicircle at higher frequencies corresponding to kinetic control and a straight line at lower frequencies corresponding to mass-transfer control. The impedance data for each sample do confirm the trends obtained by cyclic voltammetry. The slope of the straight line at lower frequency in the Nyquist plots remains close to one, reaffirming semi-infinite planar diffusion. Compared to other samples, the decrease in the diameter of semi-circle for sample **4** can be explained by decrease in film resistance, which further confirms increase in its permeability as explained by cyclic voltammetry. When mercaptoundecanoic acid (MUA) stabilized gold nanoparticles are adsorbed layer-by-layer with poly(L-arginine), the films have shown a higher permeability for $[Fe(CN)_6]^{3-/4-}$ couple at increasing layers.[51] The authors describe that the negative COO^- charge becomes further away from nanoparticle surface which in turn helps reduce the

repulsion between the redox species and negatively charged NPs. However, in $(PMo_{12}|PDDA)_{10}$ samples, the change in the microstructure of the films causes enhanced diffusion. The double layer capacitance C_d depends upon the dielectric and insulating features at the interface of electrolyte and electrode. A decrease in C_d for films at higher surface coverage (sample **4**) is observed. An apparent increase in the diffusion coefficient for sample **4** is observed as compared with other samples (Table 2). Thus, high ionic strengths of dipping solutions may induce high porosity in the films that tend to demonstrate enhanced diffusion of redox species.

Microstructure interpretation of ion transfer in LbL films. In previous work we have predicted two different micro-structures for POM films prepared with dipping solutions of different ionic strengths and concentrations. At lower ionic strengths and concentrations, the multilayer films are predicted to observe a stratified structure owing to the flat, train configuration adapted by PDDA chains (Figure 11.1). At higher ionic strengths and concentrations, PDDA chains adapt a loop and tail configuration that allows the formation of a more porous structure into which larger amount of POM clusters could occupy if available (Figure 11.2). However, along with the variation in porosity of the films we have also varied the charge on the terminating layer. Thus, we need to consider the microstructure of the films as well as the electrostatic forces at the interface tandem while explaining ionic diffusion. For the films with stratified structure, the ionic diffusion would largely depend upon the thickness of the overall film,[66] loading of POMs and finally the electrostatic attraction/repulsion at film-electrolyte interface.[38] Due to lesser porosity, ionic diffusion in such films would also depend upon the surface coverage of the film itself.[58] However, for porous microstructure, each pore inside the film can be imagined as an empty hole surrounded by a cluster of negatively charged POMs rendering a highly negative electric field on the outer edge of the hole. Thus, it would be increasingly difficult for a negatively charged redox ion to diffuse through a multilayer assembly by overcoming the repulsive effect on each pore. Meanwhile, it would be easier for a positively charged redox-probe to diffuse through such a hole. The amount of electrostatic attraction/repulsion inside the film would largely depend on the amount of POM loaded and available porosity of the film. For example, while comparing samples **2** and **4** one can imagine a microstructure with higher loadings of POM in sample **4** with a high porosity as compared to sample **2**. Thus, the electrostatic attraction/repulsion between POM clusters in the film and redox ions for sample **4** should be higher than sample **2**. Overall, the electrostatic forces at the interface as well as within the films would play a role in diffusion of porous films.

5. Conclusion

Results obtained from this study contain information for mass transfer through thin membranes. A model developed for membrane with particle components has broader applications. The conditions considered in this study can be easily applied to many situations in both industry and basic science. Here, we are able to develop a modified Randle's circuit equivalent to calculate redox species diffusion coefficients through layer-by-layer thin films deposited on electrodes. The films generally show Nyquist plots with a Warburg line slope ~ 1. From the diffusion coefficient calculations, it appears that using high ionic strength solutions would not help greatly in achieving higher ionic diffusion in the case of POM films. However, the ionic strength and concentrations of the dipping

solutions also influence the ionic diffusion of the films. For electronic diffusion, higher ionic strength solutions provide a better loading of POMs, which in turn help in enhancing the electronic conduction.

6. References

1. G. Decher, Science **277**, 1232–1237 (1997).
2. J. B. Schlenoff, H. Ly, and M. Li, J. Am. Chem. Soc. **120**, 7626–7634 (1998).
3. S. T. Dubas and J. B. Schlenoff, Macromolecules **32**, 8153–8160 (1999).
4. J. B. Schlenoff and S. T. Dubas, Macromolecules **34**, 592–598 (2001).
5. H. W. Jomaa and J. B. Schlenoff, Macromolecules **38**, 8473–8480 (2005).
6. G. B. Sukhorukov, A. A. Antipov, A. Voigt, E. Donath, and H. Möhwald, Macromol. Rapid Commun. **22**, 44–46 (2001).
7. J. H. Dai, A. M. Balachandra, J. I. Lee, and M. L. Bruening, Macromolecules **35**, 3164–3170 (2002).
8. A. M. Balachandra, J. H. Dai, and M. L. Bruening, Macromolecules **35**, 3171–3178 (2002).
9. M. D. Sullivan and M. L. Bruening, J. Am. Chem. Soc. **123**, 11805–11806 (2001).
10. L. Krasemann and B. Tieke, Langmuir **16**, 287–290 (2000).
11. W. Jin, A. Toutianoush, and B. Tieke, Langmuir **19**, 2550–2553 (2003).
12. J. Schmitt, T. Grünewald, G. Decher, P. S. Pershan, K. Kjaer, and M. Lösche, Macromolecules **26**, 7058–7063 (1993).
13. M. Lösche, J. Schmitt, G. Decher, W. G. Bouwman, and K. Kjaer, Macromolecules **31**, 8893–8906 (1998).
14. T. R. Farhat and J. B. Schlenoff, Langmuir **17**, 1184–1192 (2001).
15. H. H. Rmaile, T. R. Farhat, and J. B. Schlenoff, J. Phys. Chem. B **107**, 14401–14406 (2003).
16. T. R. Farhat and J. B. Schlenoff, J. Am. Chem. Soc. **125**, 4627–4636 (2003).
17. S. T. Dubas, T. R. Farhat, and J. B. Schlenoff, J. Am. Chem. Soc. **123**, 5368–5369 (2001).
18. J. Pozuelo, E. Riande, E. Saiz, and V. Compañ, Macromolecules **39**, 8862–8866 (2006).
19. A. A. Antipov, G. B. Sukhorukov, and H. Möhwald, Langmuir **19**, 2444–2448 (2003).
20. A. Fery, B. Schöler, T. Cassagneau, and F. Caruso, Langmuir **17**, 3779–3783 (2001).
21. I. Rubinstein and I. Rubinstein. J. Phys. Chem. **91**, 235–241 (1987).
22. B. Lindholm-Sethson, Langmuir **12**, 3305–3314 (1996).
23. J. J. Harris, P. M. DeRose, and M. L. Bruening, J. Am. Chem. Soc. **121**, 1978–1979 (1999).
24. M. Zhao, Y. Zhou, M. L. Bruening, D. E. Bergbreiter, and R. M. Crooks, Langmuir **13**, 1388–1391 (1997).
25. S. A. Merchant, D. T. Glatzhofer, and D. W. Schmidtke, Langmuir **23**, 11295–11302 (2007).
26. R. N. Vyas and B. Wang, Electrochem. Commun. **10**, 416–419 (2008).
27. R. P. Janek, W. R. Fawcett, and A. Ulman, Langmuir **14**, 3011–3018 (1998).
28. J. J. Harris and M. L. Bruening, Langmuir **16**, 2006–2013 (2000).
29. S. Han and B. Lindholm-Sethson, Electrochim. Acta **45**, 845–853 (1999).
30. V. Pardo-Yissar, E. Katz, O., Lioubashevski, and I. Willner, Langmuir **17**, 1110–1118 (2001).
31. W. Zhao, J. J. Xu, C. G. Shi, and H. Y. Chen, Langmuir **21**, 9630–9634 (2005).
32. R. Pei, X. Cui, X. Yang, and E. Wang, Biomacromolecules **2**, 463–468 (2001).

33. N. Kohli, D. Srivastava, J. Sun, R. J. Richardson, I. Lee, and R. M. Worden, Anal. Chem. **79**, 5196–5203 (2007).
34. W. Sun, R. Gao, and K. Jiao, J. Phys. Chem. B. **111**, 4560–4567 (2007).
35. F. Battaglini, E. J. Calvo, C. Danilowicz, and A. Wolosiuk, Anal. Chem. **71**, 1062–1067 (1999).
36. F. Huguenin, M. Ferreira, V. Zucolotto, F. C. Nart, R. M. Torresi, O. N. Oliveira, Jr. Chem. Mater. **16**, 2293–2299 (2004).
37. M. G. Friedrich, V. U. Kirste, J. Zhu, R. B. Gennis, W. Knoll, R. L. C. Naumann, J. Phys. Chem. B. **112**, 3193–3201 (2008).
38. M. Chirea, V. García-Morales, J. A. Manzanares, C. Pereira, R. Gulaboski, and F. Silva, J. Phys. Chem. B. **109**, 21808–21817 (2005).
39. J. O'M. Bockris, B. E. Conway, and R. E. White, Modern Aspects of Electrochemistry No 14; Plenum Press: New York, 1982; Chapter 2.
40. F. Sundfors, J. Bobacka, A. Ivaska, and A. Lewenstam, Electrochim. Acta **47**, 2245–2251 (2002).
41. P. Suresh, and V. Lakshminarayanan, Langmuir **23**, 1548–1554 (2007).
42. M. Tagliazucchi, D. Grumelli, and E. J. Calvo, Phys. Chem. Chem. Phys. **8**, 5086–5095 (2006).
43. S. Tian, J. Liu, T. Zhu, and W. Knoll, Chem. Mater. **16**, 4103–4108 (2004).
44. J. Zhao, C. R. Bradbury, and D. J. Fermín, J. Phys. Chem. C. **112**, 6832–6841 (2008).
45. H. Zhang, H. Lu, and N. Hu, J. Phys. Chem. B. **110**, 2171–2179 (2006).
46. N. A. Galiote, A. J. F. Carbvalho, and F. Huguenin, J. Phys. Chem. B. **110**, 24612–24620 (2006).
47. N. Gu., D. Wei, L. Niu and A. Ivaska, Electrochim. Acta **51**, 6038–6044 (2006).
48. L. Su, F. Gao, and L. Mao, Anal. Chem. **78**, 2651–2657 (2006).
49. S. V. P. Barreira, V. García-Morales, C. M. Pereira, J. A. Manzanares, and F. Silva, J. Phys. Chem. B. **108**, 17973–17982 (2004).
50. T. H. Silva, V. García-Morales, C. Moura, J. A. Manzanares, and F. Silva, Langmuir **21**, 7461–7467 (2005).
51. M. Chirea, C. M. Pereira, and F. Silva, J. Phys. Chem. C. **111**, 9255–9266 (2007).
52. H. O. Finklea, D. A. Snider, J. Fedyk, E. Sabatani, Y. Gafni, and I. Rubinstein, Langmuir **9**, 3660–3667 (1993).
53. A. J. Bard and L. R. Faulkner, Electrochemical Methods; Wiley: New York, 2000; Chapter 10.
54. T. R. Farhat and P. T. Hammond, Chem. Mater. **18**, 41–49 (2006).
55. N. A. Kotov, in Multilayer Thin Films: Sequential Assembly of Nanocomposite Materials; G. Decher and J. B. Schlenoff, Eds.; Wiley-VCH: Weinheim, Germany, 2003; Chapter 8.
56. N. Toshima and T. Yonezawa, New J. Chem. 1179–1201 (1998).
57. K. Y. Chan, J. Ding, J. Ren, S. Cheng, and K. Y. Tsang, J. Mater. Chem. **14**, 505–516 (2004).
58. A. S. K. Hashmi and G. J. Hutchings, Angew. Chem. Int. Ed. **45**, 7896–7936 (2006).
59. M. Sadakane and E. Steckhan, Chem. Rev. **98** 219–37 (1998).
60. B. Wang, R. N. Vyas, and S. Shaik, Langmuir **23**, 11120–11126 (2007).
61. E. Barsoukov and J. R. Macdonald, Impedance Spectroscopy; John Wiley and Sons: New York, 2005; Chapter 1.
62. W. Cheng, S. Dong, and E. Wang, Chem. Mater. **15** 2495–2501 (2003).

63. J. Qiu, H. Peng, R. Liang, J. Li, and X. Xia, Langmuir **23** 2133–2137 (2007).
64. V. P. Menon and C. R. Martin, Anal. Chem. **67**, 1920–1928 (1995).
65. O. Chailapakul and R. M. Crooks, Langmuir **11**, 1329–1340 (1995).
66. M. K. Park, D. C. Lee, Y. Liang, G. Lin, and L. Yu, Langmuir **23**, 4367–4372 (2007).

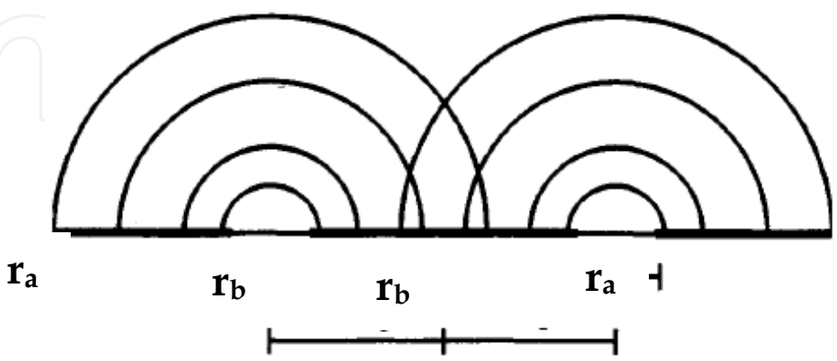

Fig. 1. Microarray parameters and diffusion profiles. Note: $\mathbf{r_a}$ is the radius of the microelectrode site and $\mathbf{r_b}$ is the radius of the inactive area surrounding the microelectrode site. Diffusion layers indicated by semicircles are isolated at short times (high frequencies) and overlapped at long times (low frequencies).

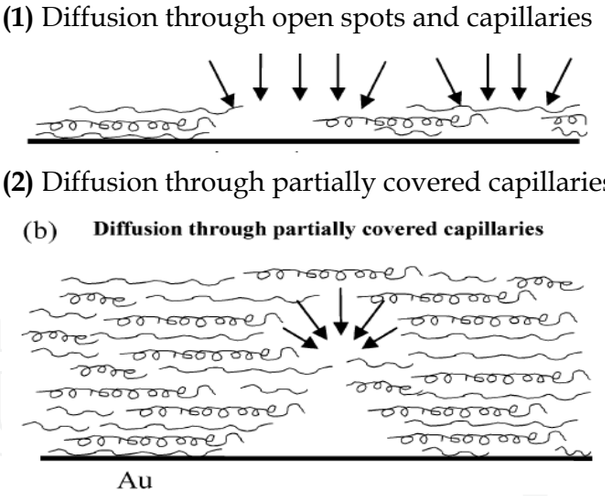

Fig. 2. Electrochemically active site configuration at two stages of film growth and their associated diffusion profiles.

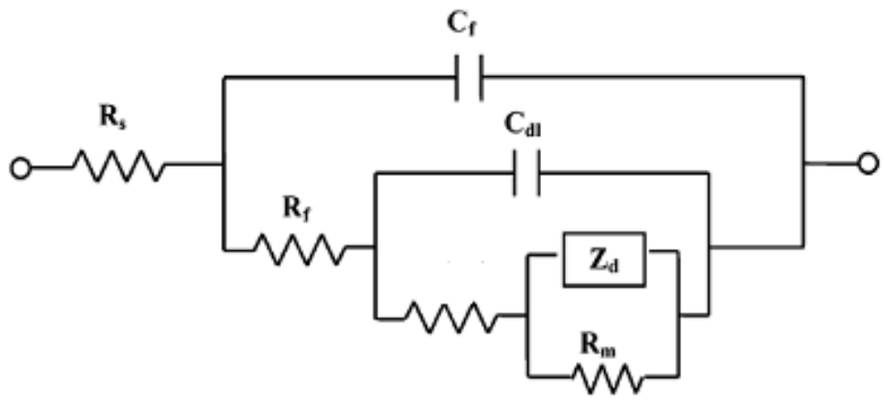

Fig. 3. Equivalent circuit for the PEM-modified electrode. Note: R_s is the solution resistance, C_f is the film capacitance, R_f is the film resistance, C_{dl} is the double layer capacitance associated with metal surface, R_{ct} is the apparent charge-transfer resistance, R_m is the resistance representing Ohmic conduction in the film, and Z_d is the diffusion impedance.

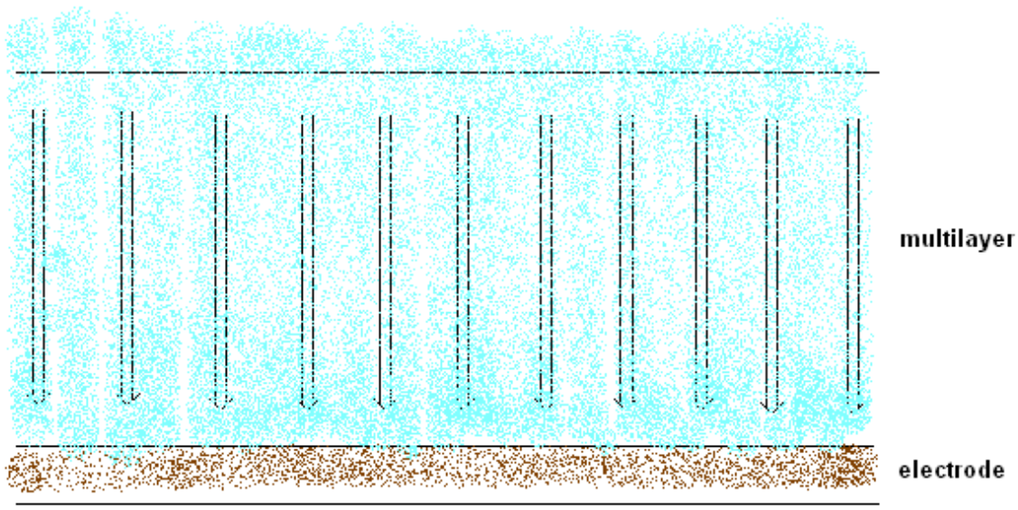

Fig. 4. Diffusion paths across the homogeneous membrane when the number of layers is large.

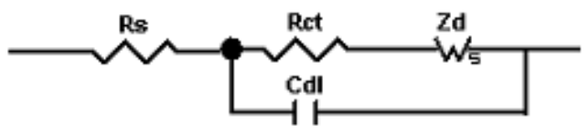

Fig. 5. A conventional Randle's circuit. R_s is solution resistance, R_{ct} is charge transfer resistance, Z_d is the Warburg impedance, and C_{dl} is the double layer capacitance.

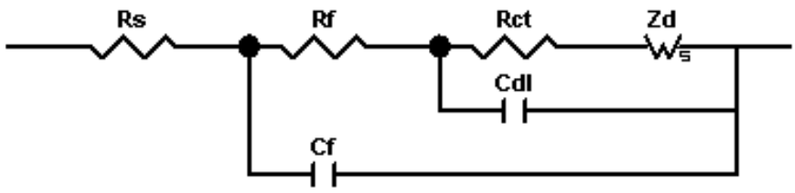

Fig. 6. A modified Randle's equivalent circuit. R_s is solution resistance, R_{ct} is charge transfer resistance, R_f is the film resistance, Z_d is the Warburg impedance, C_f is the film capacitance, and C_{dl} is the double layer capacitance.

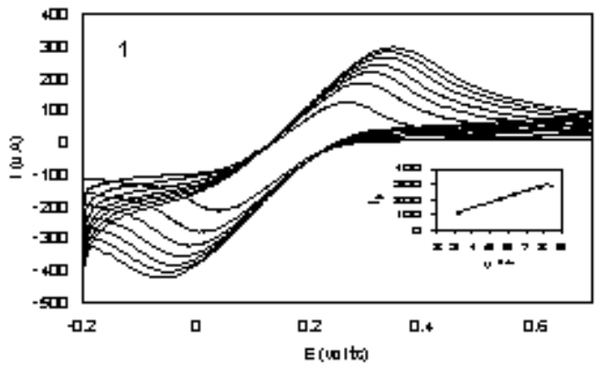

Fig. 7. Cyclic voltammograms for $(PMo_{12}|PDDA)_{10}$ sample **1** at scan rates 10, 20, 30, 40, 50, 60, 70 mV $\cdot s^{-1}$. Inset shows the anodic peak current vs square root of scan rate.

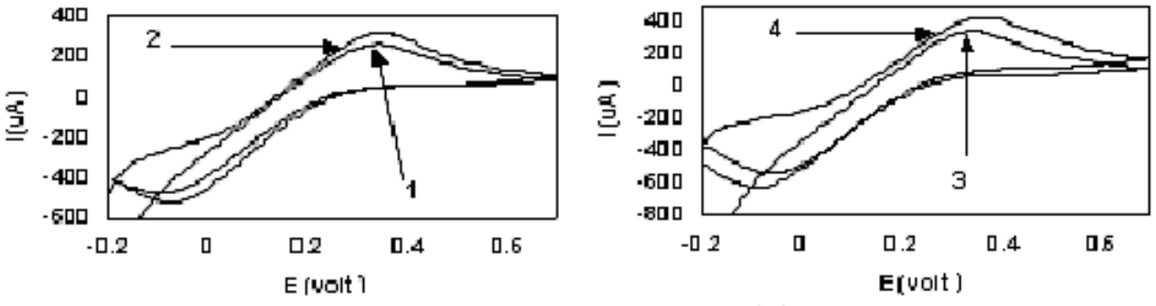

Fig. 8. Cyclic voltammograms obtained at 100 mV $\cdot s^{-1}$ in presence of (0.005 M $[Fe(CN)_6]^{3-/4-}$ in 0.025 M Na_2HPO_4, pH 6.3) for $(PMo_{12}|PDDA)_{10}$ films: a) samples **1** and **2**; b) samples **3** and **4** in Table 1.

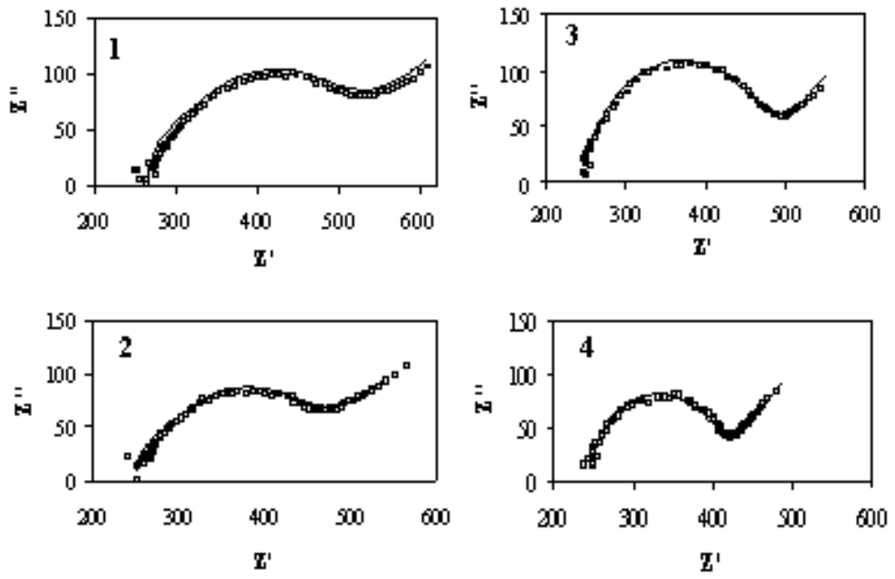

Fig. 9. Electrochemical impedance spectra (0.005 M $[Fe(CN)_6]^{3-/4-}$ in 0.025 M Na_2HPO_4, pH 6.3) for $(PMo_{12}|PDDA)_{10}$ films. Frequency range: 1–10^5 Hz. Sinusoidal Voltage: 10 mV. The dc potential: 220 mV. The electrode was immersed 5 min prior to data acquisition. (□) Experimental curve; (—) Fitting curve.

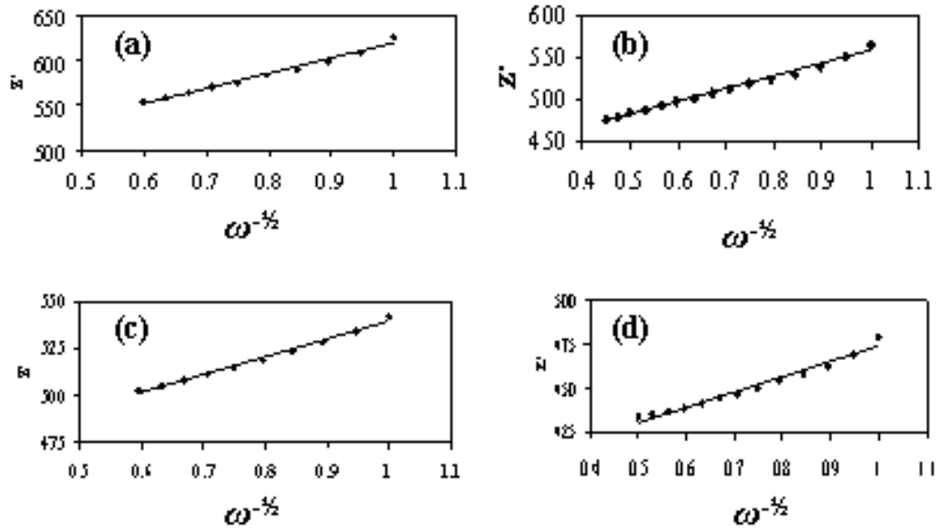

Fig. 10. Z' vs. $\omega^{-1/2}$ plots for samples: (a) **1**, (b) **2**, (c) **3**, and (d) **4**. Low frequency range selected for Warburg line from the Nyquist plot.

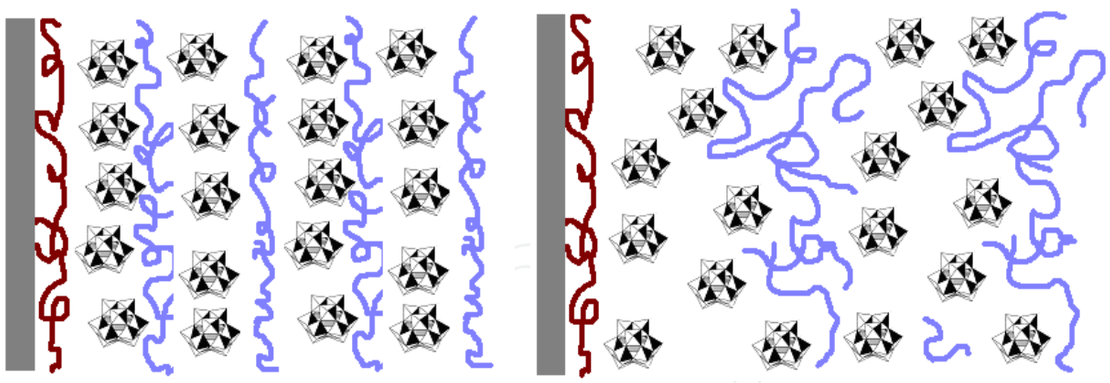

(1) (2)

Fig. 11. Proposed (POM | PDDA)$_{10}$ multilayer microstructures: **(1)** under low ionic strength, **(2)** under high ionic strength. Legends: gray slab, substrate; brown chains, PEI; polyhedrons, POM; blue chains, PDDA.

sample	PMo_{12} (mM)	pH of solutions	NaCl (M)
1	0.1	3.3	0
2	0.1	3.3	0.1
3	10.0	2.0	0
4	10.0	2.0	0.1

Table 1. Preparation Parameters used in Layer-by-Layer Construction of (PMo_{12} | PDDA)$_{10}$ Films.

sample	R_s $\Omega \cdot cm^2$	R_{ct} $\Omega \cdot cm^2$	R_f $\Omega \cdot cm^2$	C_f $\mu F \cdot cm^{-2}$	C_{dl} $\mu F \cdot cm^{-2}$	D $10^{-7}\ cm^2 \cdot s^{-1}$
1	265	105	115	7.8	2.4	0.8
2	250	100	90	8.0	2.5	1.3
3	245	100	120	8.0	10.0	2.9
4	245	95	60	8.0	3.0	4.2

Table 2. Parameter Values Obtained by Fitting the Impedance Data of (PMo_{12} | PDDA)$_{10}$ Films (Samples **1-4**) from Table 1 to Modified Randle's Equivalent Circuit in Figure 6.

Polymer Thin Films

Edited by Abbass A Hashim

ISBN 978-953-307-059-9
Hard cover, 324 pages
Publisher InTech
Published online 01, April, 2010
Published in print edition April, 2010

This book provides a timely overview of a current state of knowledge of the use of polymer thin film for important technological applications. Polymer thin film book covers the scientific principles and technologies that are necessary to implement the use of polymer electronic device. A wide-ranging and definitive coverage of this emerging field is provided for both academic and practicing scientists. The book is intended to enable readers with a specific background, e.g. polymer nanotechnology, to become acquainted with other specialist aspects of this multidisciplinary field. Part A of the book covers the fundamental of the key aspect related to the development and improvement of polymer thin film technology and part B covers more advanced aspects of the technology are dealt with nano-polymer layer which provide an up-to-date survey of current research directions in the area of polymer thin film and its application skills.

InTech Europe
University Campus STeP Ri
Slavka Krautzeka 83/A
51000 Rijeka, Croatia
Phone: +385 (51) 770 447
Fax: +385 (51) 686 166
www.intechopen.com

InTech China
Unit 405, Office Block, Hotel Equatorial Shanghai
No.65, Yan An Road (West), Shanghai, 200040, China
中国上海市延安西路65号上海国际贵都大饭店办公楼405单元
Phone: +86-21-62489820
Fax: +86-21-62489821

IntechOpen